Buckling of swelling gels

T. Mora[a] and A. Boudaoud

Laboratoire de Physique Statistique de l'École Normale Supérieure, 24, rue Lhomond, 75231 Paris Cedex 05, France

Abstract. The patterns arising from the differential swelling of gels are investigated experimentally and theoretically as a model for the differential growth of living tissues. Two geometries are considered: a thin strip of soft gel clamped to a stiff gel, and a thin corona of soft gel clamped to a disk of stiff gel. When the structure is immersed in water, the soft gel swells and bends out of plane leading to a wavy periodic pattern whose wavelength is measured. The linear stability of the flat state is studied in the framework of linear elasticity using the equations for thin plates. The flat state is shown to become unstable to oscillations above a critical swelling rate and the computed wavelengths are in quantitative agreement with the experiment.

PACS. 46.32.+x Static buckling and instability – 61.41.+e Polymers, elastomers, and plastics – 87.18.La Morphogenesis – 68.35.Gy Mechanical properties; surface strains

1 Introduction

Living organisms are full of fascinating complex patterns. One might wonder about the physical mechanisms at stake as well as their relevance. Although a tissue is obviously an elastic solid, the role of mechanical stresses in morphogenesis was not investigated from a physical perspective until recently. On the one hand, they were shown to be important in phyllotaxis (the arrangement of leaves in plants) [1, 2], in the wrinkling of leaves [3,4], in the selection of cell sizes [5], as well as in the development of embryos [6]. On the other hand, a theoretical framework was introduced to study the instabilities occurring in the growth of elastic bodies [7].

At first sight, it is difficult to find physical systems allowing the investigation of growth. The tearing of plastic sheets as in [3] generates beautiful self-similar buckling patterns, but gives little control over the growth rate. However, some polymeric gels can undergo huge volume changes when submitted to external stimuli such as variations in temperature, pH, osmotic pressure [8,9], electric field [10] or light [11]. Strictly speaking, such a gel does not grow but swells by absorbing water while its elastic modulus decreases. Another important difference with living tissues is that, in such gels, there is no feedback of mechanical stresses on the rate of swelling/growth. A number of studies (see [12] for a review) have been devoted to the instabilities of swelling or deswelling gels, such as

the folding of the surface of swollen gels clamped to hard substrates and the subsequent formation of a network of cusp lines [13–17].

In this article we are concerned with the instabilities occurring in the differential swelling of gels. Our main motivation is to design physical counterparts to growing tissues and to determine the generic patterns emerging in the growth/swelling of elastic bodies. We use thin gel plates made by assembling two gels with different elastic and swelling properties, we investigate the patterns resulting from the swelling of the plates. This procedure could also be a method to generate micro-patterns in microscopic films or layered structures. In previous studies on such micro-systems, a number of methods were used to produce the stresses that generated the buckling patterns: cooling [18,19], swelling in a solvent [20], evaporation [21], spinodal decomposition [22] or thermal annealing [23].

Here we investigate the buckling patterns induced by the swelling of a soft-gel plate clamped to a nonswelling stiff-gel plate. First, in Section 2, we describe the experimental procedure and give our first observations. In Section 3, we introduce the theoretical framework and the linear-stability analysis. In Section 4, we compare quantitatively the experimental and theoretical results. We eventually give a discussion and some perspectives in Section 5.

2 The experiment

Our goal was to design an experiment to study the differential swelling of gels. We chose to assemble two thin flat gels having different elastic and swelling properties in

[a] *Present address*: LPTMS, Université Paris-Sud, Centre scientifique d'Orsay, 15 rue Georges Clémenceau, 91405 Orsay cedex, France; e-mail: boudaoud@lps.ens.fr

Table 1. Composition and properties of the gels used in the experiment. Concentrations are given in mmol L^{-1}. The length ratio corresponds to the ratio of a free-gel dimensions before and after swelling. E is the elastic modulus of the gel.

	(I)	(II)
[AA + BISAA]	720	2880
BISAA : AA ratio	1 : 37.5	1 : 19
[SA]	46–183	0
Length ratio	150%–180%	106%
E (Pa)	$5.0 \cdot 10^3$	$3.2 \cdot 10^5$

order to obtain a gel plate whose properties vary along the width (and are constant along the thickness). Polyacrylamide gels are suitable as they swell when immersed in water whereas their swelling and elastic properties can be tuned independently.

We prepared our gels as in [8,9,24]. A mixture of acrylamide (AA) and N,N′-methylenebisacrylamide (BISAA) is dissolved with sodium acrylate (SA) in distilled water. The polymerization is initiated by ammonium persulfate (PA) and is catalysed with N,N,N′,N′-tetramethylenediamine (TEMED) (0.3% in volume). The composition of the gels is given in Table 1. (Other compositions were investigated qualitatively and the corresponding results are mentionned in Sect. 4.3.) In these conditions, gelation generally occurs within one minute after the addition of the catalyst.

The characteristics of the gel can be tuned by varying the concentrations of the components. The more concentrated (and, for the same concentration, the more concentrated in BISAA) the solution, the stiffer the gel. Likewise, the equilibrium length ratio (the ratio between a free-gel dimensions before and after swelling) can be increased by adding sodium acrylate. For the purpose of the experiment we prepared two distinct types of gel: (I) a soft and swelling gel; (II) a stiff and nonswelling gel. The elastic and swelling properties of these gels have been measured and are reported in Table 1. The elastic modulus was determined by hanging weights to the extremity of a gel plate, whereas the equilibrium length ratio was measured directly on a swollen free gel. Typically the stiff gel is two orders of magnitude stiffer than the soft one and the soft gel swells by a factor of 5 in volume.

The gelation process is performed in a thin cell composed of two glass plates separated by rubber spacers of constant thickness h (1 to 5 mm). The cell is set vertically. The spacers are used as masks shaped according to two different geometries:

– The so-called *strip geometry* consists of two thin strips of gel of respective compositions (I) and (II), clamped by their edges (see Fig. 1). To obtain this geometry, solution (II) was first poured into the cell and left for gelation. Then solution (I) was added to form a second layer of width l (typically 1 cm) and length 20 cm. In the process of gelation of the second layer, the two layers become chemically clamped to each other.
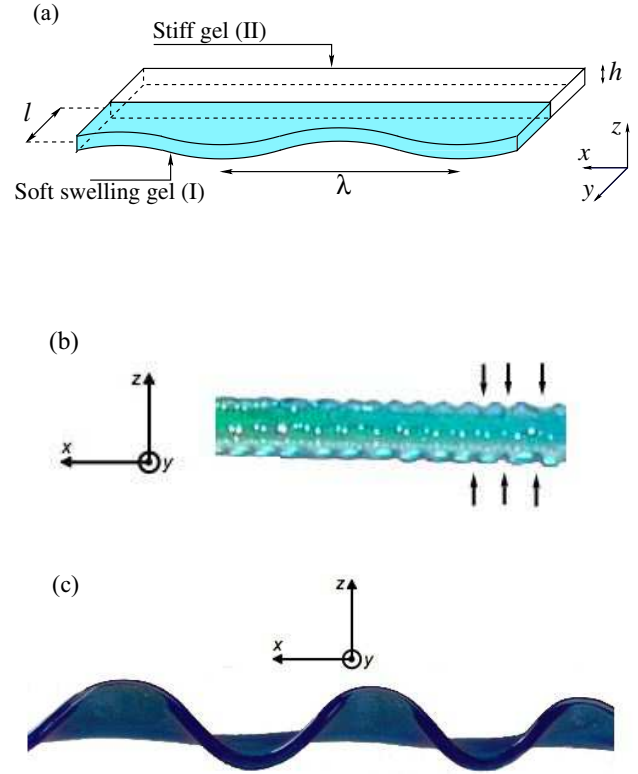
Fig. 1. The strip geometry. A strip of soft swelling gel (I) is chemically clamped to a strip of stiff nonswelling gel (II). When immersed in water, part (I) swells while part (II) does not. (a) Schematic of the experimental setting. (b) Side view (along the y-direction) in the regime with cusps. The middle plane of gel (I) remains flat while the surface of the gel becomes wavy and displays cusps (a few of which are shown by arrows). Strip of initial thickness $h = 2.25$ mm and width $l = 5$ mm. (c) Side view (along the y-direction) in the buckling regime. When swelling, the middle surface of gel (I) oscillates out of plane with a well-defined wavelength λ. Strip of initial thickness $h = 2.25$ mm and width $l = 30$ mm.

– The *corona geometry* is the axisymmetric counterpart of the strip geometry. A disk (radius r_i in the range 2–5 cm) of gel (II) is clamped to a corona (inner radius r_i, outer radius r_o in the range 2–5 cm as well) of gel (I) (see Fig. 2). We used circular masks of various radii to obtain these shapes: first the disk is made, then the cell is opened, the mask is replaced and the corona is moulded after closing back the cell.

After opening the cell, we obtain a structure made of two chemically clamped gels with different properties. Incidentally, whenever the structure is accidentally broken, the failure always occurs in the bulk of the soft part, which shows that the clamping is strong. The whole is then immersed in water for several hours until a stationary state is reached and the swelling process is complete. In both cases, the sample undergoes a mechanical buckling instability such that the soft gel is no longer flat (except for
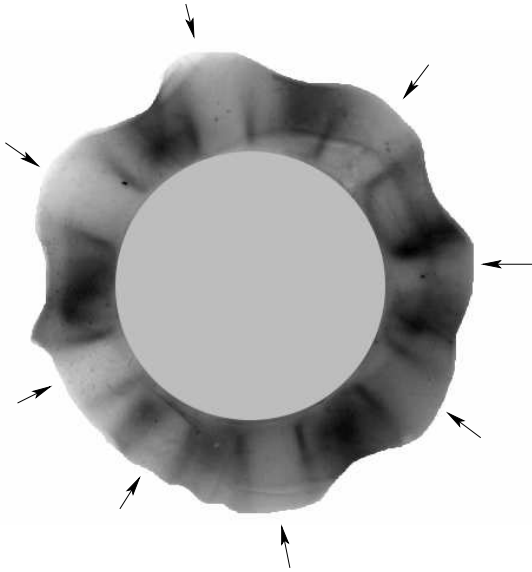
Fig. 2. The corona geometry. A corona (inner radius r_i and outer radius r_o) of soft swelling gel (I) is clamped to a disk of stiff nonswelling gel (II). When swelling, the corona becomes unstable and goes off the inital plane. The wave number is eight in this picture ($h = 1\,\text{mm}$, $r_i = 3.5\,\text{cm}$ and $r_o = 5\,\text{cm}$). The arrows indicate the crests of the swollen gel.

narrow strips —see below). This results in a wavy pattern (Figs. 1, 2) with a well-defined wavelength.

In the strip geometry, the wavelength increases with the width of the strip l. We also performed some experiments with different swelling ratios and found similar results. For a small width l no buckling occurred but we observed instead a fine pattern with regularly spaced cusps similar to those studied in [13]. In the corona geometry, the pattern is periodic and is characterised by a wave number (defined as the number of complete wavelengths) which increases with the aspect ratio r_o/r_i. A more quantitative description is delayed to Section 4.

3 Theoretical setting

We now study the patterns using a linear-stability analysis of the equations of elasticity for a flat initial state. We consider only the soft swelling part (I) of the structure, the other part (II) being considered as static as it swells by a small amount and it is very stiff. Since the gel sample is thin and flat before the instability, we can use the Foppl-von Kármán equations for thin elastic plates [25]. Material points are parametrized by their initial planar Cartesian coordinates x and y. A deformation is defined by the displacement field $(u_x(x,y), u_y(x,y), \zeta(x,y))$; u_x and u_y are the in-plane displacements along the x and y axes, respectively, whereas ζ is the transverse (off-plane) displacement. We use the framework of linear elasticity which will prove sufficient for the interpretation of the results (this restriction is discussed in the conclusion), so that the in-plane stress tensor $\sigma_{\alpha\beta}$ ($\alpha,\beta = x,y$) depends

linearly on the deformation tensor $u_{\alpha\beta}$ [25]:

$$u_{\alpha\beta} = \frac{1}{2}\left(\frac{\partial u_\alpha}{\partial x_\beta} + \frac{\partial u_\beta}{\partial x_\alpha} + \frac{\partial \zeta}{\partial x_\alpha}\frac{\partial \zeta}{\partial x_\beta}\right), \tag{1}$$

$$\sigma_{xx} = \frac{E}{1-\sigma^2}\left(u_{xx} + \sigma u_{yy}\right), \tag{2}$$

$$\sigma_{yy} = \frac{E}{1-\sigma^2}\left(u_{yy} + \sigma u_{xx}\right), \tag{3}$$

$$\sigma_{xy} = \frac{E}{1+\sigma}u_{xy}, \tag{4}$$

where $\sigma = 1/2$ is the Poisson ratio of the gel (these gels are almost incompressible). The Föppl-von Kármán equations for equilibrium [25] read

$$D\Delta^2\zeta - h\frac{\partial}{\partial x_\beta}\left(\sigma_{\alpha\beta}\frac{\partial \zeta}{\partial x_\alpha}\right) = 0, \tag{5}$$

$$\frac{\partial \sigma_{\alpha\beta}}{\partial x_\beta} = 0, \tag{6}$$

for out-of-plane bending and in-plane stretching, respectively. The bending stiffness is

$$D = \frac{Eh^3}{12(1-\sigma^2)}. \tag{7}$$

The corresponding (linearized) boundary conditions are given in the next two subsections.

3.1 The strip geometry

We now specify the formulation for the strip geometry. The reader should refer to Figure 1 for the notations. From this point onwards we use l as unit of length and $D/(hl^2)$ as unit of stress. The constraint imposed by (II) results in the compression of the swollen strip in the x-direction. We study the linear stability of the flat solution such that $\zeta = 0$. Using the boundary conditions $u_y(0,x) = 0$ at the clamped edge and $\sigma_{xx}(x,1) = 0$ at the free edge, the solution to equation (6) yields $u_x = -kx$ ($k > 0$ because the strip is compressed) and $u_y = 0$. Then the equilibrium equations reduce to

$$\Delta^2\zeta + P\frac{\partial^2\zeta}{\partial x^2} = 0, \tag{8}$$

$P = 12kl^2/h^2$ being the compressive (nondimensional) stress applied along the x-direction.

We look for periodic solutions in the form

$$\zeta(x,y) = \xi(y)\cos qx. \tag{9}$$

Using (8), $\xi(y)$ appears to be the solution of a fourth-order linear differential equation with constant coefficients. As a consequence, its solutions can be written in the form

$$\xi(y) = A\exp(imy) + B\exp(-imy)$$
$$+ C\exp(ny) + D\exp(-ny), \tag{10}$$
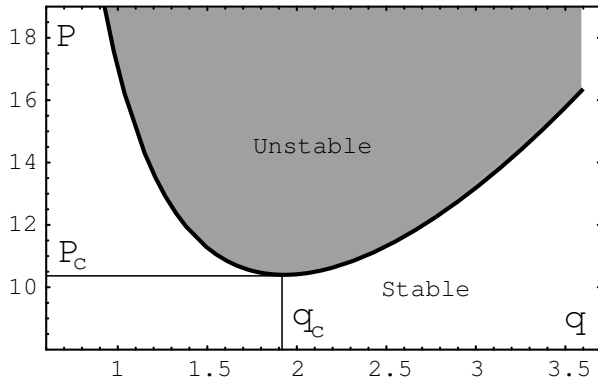
Fig. 3. The stability diagram. Nondimensional critical compressive stress P as a function of the nondimensional wave number q at the limit of stability. The flat strip is unstable (respectively stable) above the curve (respectively below the curve). The most unstable wave number corresponds to the minimum $P_c = 10.40$ and $q_c = 1.930$.

Fig. 4. Most unstable mode for an infinite flat strip of gel longitudinally compressed on one edge, as given by the solution to equation (8).

n and m being the real solutions of

$$P = \frac{(m^2 + q^2)^2}{q^2} \quad \text{and} \quad n^2 - m^2 = 2q^2. \quad (11)$$

The boundary equations on the clamped ($y = 0$) and free ($y = 1$) edges read [25]

$$\xi(0) = 0, \qquad \xi''(1) - \sigma q^2 \xi(1) = 0,$$
$$\xi'(0) = 0, \qquad -\xi^{(3)}(1) + (2 - \sigma)q^2 \xi'(1) = 0.$$

These conditions can be viewed as a system of 4 linear equations with the four unknowns A, B, C, D. A nonzero solution ζ exists if and only if the determinant is zero, which occurs for a certain $P(q)$. This curve is shown in Figure 3. It corresponds to the marginal stability, *i.e.* the smallest value of the compressive stress P for which a wave number q can exist and so it becomes unstable.

The first wave number q_c to become unstable corresponds to the minimum of $P(q)$. This yields the critical wave number $q_c = 1.390$ and the threshold on compression $P_c = 10.40$. Using dimensional quantities, the corresponding wavelength and critical length ratio read

$$\lambda = \frac{2\pi}{q_c} = 3.256\,l, \qquad k_c = \frac{P_c h^2}{12 l^2} = 0.867 \frac{h^2}{l^2}. \quad (12)$$

A 3-dimensional representation of the corresponding solution $\zeta(x, y)$ of (8) is shown in Figure 4. Note that, when comparing to the experimental wavelengths, we implicitly assume that the compression is near its threshold. This is another limitation which is discussed in the conclusion.

3.2 The corona geometry

We now proceed to the same analysis for the corona geometry. The swollen corona ($r_i < r < r_o$) is supposed to be radially pulled at the inner edge so that its inner radius shrinks to fit the radius of the unswollen disk. Note that r_i and r_o are the dimensions of the corona *if it had swollen unconstrained*. Although neither of these radii can be measured directly, their ratio r_i/r_o is the same as before swelling. From this point onwards we use the outer radius r_o as unit of length and $D/(hr_o^2)$ as unit of stress. In these reduced units, r_i is the aspect ratio of the corona before the swelling.

We first need the stress field in the flat corona as resulting from the tension at the inner radius. We look for a solution of (6) in the form

$$u_r = ar + \frac{b}{r}, \qquad u_\theta = 0. \quad (13)$$

r and θ are the standard polar coordinates. The boundary conditions are $u_r(r = r_i) = -\beta$ (displacement to fit the unswollen gel) at the inner edge and $\sigma_{rr}(r = 1) = 0$ (stress free) at the outer edge. The problem has now one single degree of freedom β. We obtain a stress tensor of the form

$$\sigma_{rr} = -\alpha\left(1 - \frac{1}{r^2}\right), \qquad \sigma_{\theta\theta} = -\alpha\left(1 + \frac{1}{r^2}\right). \quad (14)$$

The number α being proportional to β is chosen as the swelling control parameter. The balance of moments (5) reduces to

$$\Delta^2\zeta + \alpha\Delta\zeta + \frac{\alpha}{r^2}\left(-\frac{\partial^2\zeta}{\partial r^2} + \frac{3}{r}\frac{\partial\zeta}{\partial r} + \frac{1}{r^2}\frac{\partial^2\zeta}{\partial\theta^2}\right) = 0, \quad (15)$$

with

$$\Delta\zeta = \frac{\partial^2\zeta}{\partial r^2} + \frac{1}{r^2}\frac{\partial^2\zeta}{\partial\theta^2} + \frac{1}{r}\frac{\partial\zeta}{\partial r}. \quad (16)$$

At the clamped edge ($r = r_i$), the boundary conditions read

$$\xi = 0,$$
$$\frac{\partial\xi}{\partial r} = 0, \quad (17)$$

whereas at the free edge ($r = 1$),

$$-\frac{\partial}{\partial r}\Delta\zeta + (1 - \sigma)\frac{1}{r^3}\left(\frac{\partial^2\zeta}{\partial\theta^2} - r\frac{\partial^3\zeta}{\partial r\partial\theta^2}\right) = 0,$$
$$\Delta\zeta + (\sigma - 1)\frac{1}{r^2}\left(\frac{\partial^2\zeta}{\partial\theta^2} + r\frac{\partial\zeta}{\partial r}\right) = 0. \quad (18)$$

We look for periodic solutions to (15) in the form

$$\zeta(r, \theta) = \xi(r)\cos m\theta, \quad (19)$$

where the wave number m is an integer. We find a fourth-order linear equation in $\xi(r)$.

We first compute a basis of the 2-dimensional space formed by the solutions satisfying the conditions at the
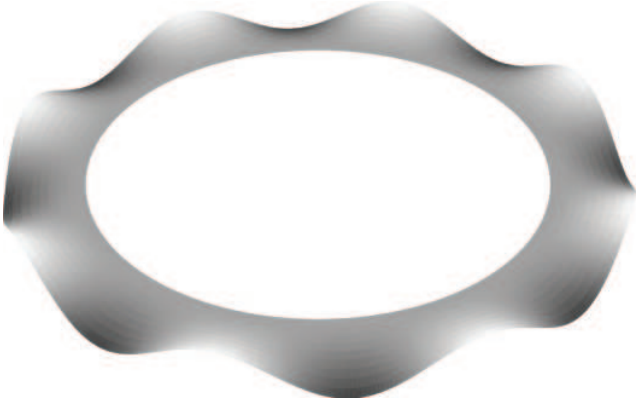
Fig. 5. Most unstable mode for a flat corona of gel with radial tension at the inner radius. The aspect ratio (inner radius/outer radius) is 0.74. The selected wave number is $m = 8$.

inner boundary (17). To proceed, we solve the differential equation with initial conditions

$$(\xi(r_i), \xi'(r_i), \xi''(r_i), \xi'''(r_i)) = \begin{cases} (0, 0, 1, 0), \\ (0, 0, 0, 1), \end{cases}$$

using a Runge-Kutta algorithm, so that we find the basis ξ_1, ξ_2. A nonzero linear combination of ξ_1 and ξ_2 verifying the conditions at the outer boundary (18) exists only for a certain $\alpha(m, r_i)$, which we compute numerically. Using the same argument as in the strip geometry, we choose $m(r_i)$ for which $\alpha(m, r_i)$ is minimum. Thus we obtain the wave number m as a function of the aspect ratio r_i. Figure 5 shows the solution $\xi(r, \theta)$ of (15) with the aspect ratio $r_i/r_o = 0.74$ for which $m = 8$.

We also tested the $r_i \to 1$ limit of our numerical calculation. In this limit, the corona geometry should reduce to the strip geometry, as the curvature of the interface between the two gels vanishes. The wavelength reads

$$\frac{\lambda}{l} \approx \frac{\pi}{m} \frac{1 + r_i}{1 - r_i}. \tag{20}$$

For $r_i = 0.9999$, we obtained indeed $\lambda/l = 3.255$ in agreement with (12).

4 Results

4.1 The strip geometry

The two geometrical parameters are the width l of the swollen strip, and the thickness h of the gel before swelling. We plotted our observations in Figure 6, along with the analytical result (12). The gel goes off the plane for $l > l_c \sim 2h$. The wavelength of the instability increases with l, and is approximately linear with l in the limit of small thickness $h \ll l$, in agreement with the theoretical result. Indeed, the theoretical approach uses the theory of thin plates, *i.e.* it assumes that $l \gg h$. For $l < l_c$, instability patterns are observed on the surface of the swollen gel
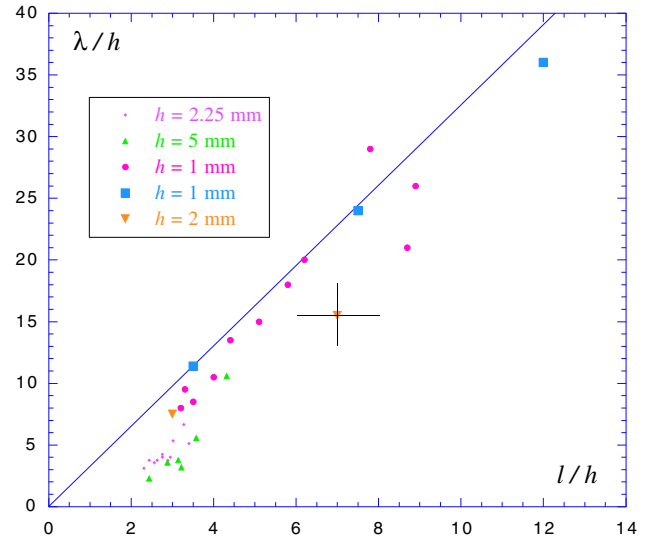
Fig. 6. Instability wavelength λ as a function of the width l of the swollen strip. The measurements are normalised by the thickness h of the gel and typical error bars are shown. Off-plane instability is observed for $l > l_c \sim 2h$. For $l < l_c$, cusped patterns appear on the surface of the swollen gel. The line corresponds to the theoretical result $\lambda = 3.256\,l$ (Eq. (12), valid for $l \gg h$).
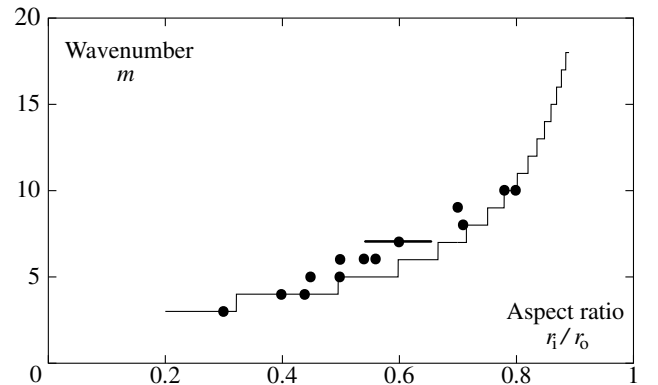
Fig. 7. Wave number m of the instability as a function of the aspect ratio (inner radius r_i/outer radius r_o) before swelling. Circles: experimental results (a typical error bar is shown). Line: theoretical result.

(Fig. 1), whereas the middle plane of the gel remains flat. They consist in regularly spaced cusps similar to those observed in [13].

4.2 The corona geometry

In the corona geometry experiment, the thickness h was fixed to 1 mm, and the inner and outer radii were varied from 20 mm to 50 mm. Thus, the theory of thin plates remains valid, which allows a direct comparison between experimental and analytical results (Fig. 7). The wave number m increases with the aspect ratio r_i/r_o, in quantitative agreement with the theoretical predictions.

4.3 Other observations

We also varied the other experimental parameters although not systematically. Concerning the composition of the soft gel, we varied the content in sodium acrylate to change the equilibrium length ratio (115% to 180%) with no noticeable alteration of the patterns and the wavelengths, which supports the assumption that the wavelengths depend very little on the applied stresses. We mainly investigated the situation such that the stiff gel is much stiffer than the soft gel —the results do not depend on the width of the hard gel. If this condition is relaxed either by softening the hard gel or stiffening the soft gel, we observed the oscillations to penetrate the hard gel. In this case, we expect the wavelength to increase with the width of the system.

5 Conclusion

To summarise, we showed that the swelling of thin soft-gel plates clamped to a stiff gel leads to a buckling instability. A linear-stability analysis yields a prediction for the pattern wavelengths in quantitative agreement with the experiment. These wavelengths are mainly determined by the in-plane geometry of the thin gel. Our analysis is restricted by two main limitations.

On the one hand, we used the most unstable modes to predict the wavelengths at the instability threshold, whereas the experimental conditions are far above this threshold. For instance, in the strip geometry $k \sim 0.5$ as given by Table 1 while the threshold is estimated as $k_c \sim h^2/l^2 \sim 10^{-2}$. However, standard weakly nonlinear analysis generally yields almost the same wavelengths [26]. On the other hand, we used the framework of linear elasticity while the equilibrium length ratios are large and the deformations are finite. Moreover, the flat base state is anisotropic: for instance, in the strip geometry, the gel has swollen differently along the two in-plane directions, so that the elastic modulus is not strictly the same in these two directions. The small discrepancies between the experimental and theoretical wavelengths might be ascribed to either of these two limitations.

A suggestion for future research stems from the second limitation, which we believe to be the main source of descrepancies. One might use the framework of nonlinear elasticity developed in [7] (for a spherical geometry) to build a more precise theory for the present experiment —this would account for large deformations and for anisotropy of the base state. On the experimental side, we have shown how to design physical counterparts to growing tissues. The main conclusion from the present study is that differential growth/swelling of thin gels/tissues naturally leads to buckling instabilities which could account for the wavy shape of the edge of certain leaves or flowers [3,4]. This experimental technique could also be used for the patterning of layered micro-structures. Other geometries are currently investigated and will be the subject of forthcoming publications.

References

1. C.R. Steele, J. Appl. Mech. **67**, 237 (2000).
2. P. Shipman, A. Newell, Phys. Rev. Lett. **92**, 168102 (2004).
3. E. Sharon, B. Roman, M. Marder, G.S. Shin, H.L. Swinney, Nature **419**, 579 (2002).
4. B. Audoly, A. Boudaoud, Phys. Rev. Lett. **91**, 086105 (2003).
5. A. Boudaoud, Phys. Rev. Lett. **91**, 018104 (2003).
6. E. Brouzès, E. Farge, Curr. Opin. Gen. Dev. **14**, 367 (2004).
7. M. Ben Amar, A. Goriely, J. Mech. Phys. Solids **53**, 2284 (2005).
8. T. Tanaka, Phys. Rev. A **17**, 763 (1978).
9. T. Tanaka, D. Fillmore, S.-T. Sun, I. Nishio, G. Swislow, A. Shah, Phys. Rev. Lett. **45**, 1636 (1980).
10. T. Tanaka, I. Nishio, S.-T. Sun, S. Ueno-Nishio, Science **218**, 467 (1982).
11. S. Juodkazis, N. Mukai, R. Wakaki, A. Yamaguchi, S. Matsuo, H. Misawa, Nature **408**, 178 (2000).
12. A. Boudaoud, S. Chaïeb, Phys. Rev. E **68**, 021801 (2003).
13. T. Tanaka, S.-T. Sun, Y. Hirokawa, S. Katayama, J. Kucera, Y. Hirose, T. Amiya, Nature **325**, 796 (1987).
14. T. Hwa, M. Kardar, Phys. Rev. Lett. **61**, 106 (1988).
15. A. Onuki, Phys. Rev. A **39**, 5932 (1989).
16. N. Suematsu, K. Sekimoto, K. Kawasaki, Phys. Rev. A **41**, 5751 (1990).
17. H. Tanaka, H. Tomita, A. Takatsu, T. Hayashi, T. Nishi, Phys. Rev. Lett. **68**, 2794 (1992).
18. N. Bowden, S. Brittain, A.G. Evans, J.W. Hutchinson, G.M. Whitesides, Nature **393**, 146 (1998).
19. N. Bowden, W.T.S. Huck, K.E. Paul, G.M. Whitesides, Appl. Phys. Lett. **75**, 2557 (1999).
20. J.S. Sharp, R.A.L. Jones, Phys. Rev. E **68**, 011801 (2002).
21. S. Joon Kwon, Jae-Gwan Park, J. Chem. Phys. **122**, 031101 (2005).
22. P.J. Yoo, K.Y. Suh, H. Kang, H.H. Lee, Phys. Rev. Lett. **93**, 034301 (2005).
23. T. Ohzono, M. Shimomura, Phys. Rev. E. **72**, 023203(R) (2005).
24. Y. Li, C. Li, Z. Hu, J. Chem. Phys. **100**, 4637 (1994).
25. L. Landau, E. Lifchitz, *Théorie de l'élasticité* (Mir, Moscou, 1990).
26. P. Manneville, *Dissipative Structures and Weak Turbulence* (Academic Press, New York, 1990).